Connection between attached eddies, friction factor, and mean-velocity profile

H. R. Anbarlooei* and F. Ramos
Department of Applied Mathematics, Institute of Mathematics, Federal University of Rio de Janeiro, Rio de Janeiro, Brazil

D. O. A. Cruz
Mechanical Engineering Program, COPPE, Federal University of Rio de Janeiro, Rio de Janeiro, Brazil

(Received 9 October 2021; accepted 10 February 2022; published 24 February 2022)

This work connects the attached eddies to the wall friction by relating the momentum transfer normal to the lower bound of the energetic range with the wall shear stress. Evidence is provided to show that this balance is the property of a specific layer, $l \approx 3\sqrt{\mathrm{Re}_\tau}$, which coincides with the smallest attached eddies. As a result, our model predicts successfully the transition of the friction factor after the Blasius regime to the extreme Reynolds numbers range, and the resulting friction equation shows the same accuracy as the well-known logarithmic laws. This transition also affects the mean velocity profile. From the developed friction equation, a mean velocity profile is derived which is in accordance with the well-known log laws. Finally, it is conjectured that for high enough Reynolds numbers, both Prandtl's 1/7 power law and the velocity profile approximate the mean velocity simultaneously, however at different distances from the wall.

DOI: 10.1103/PhysRevFluids.7.024602

I. INTRODUCTION

The Reynolds averaged momentum equation in the streamwise direction for the pipe geometry reads as

$$\frac{1}{r}\frac{d}{dr}(\overline{u_r' u_z'}) = -\frac{1}{\rho}\frac{dP}{dz} + \nu\frac{d}{dr}\left(r\frac{dU}{dr}\right), \tag{1}$$

where z and r are streamwise and radial directions, U is the streamwise averaged velocity, and u_r' and u_z' stand for the velocity fluctuations in respective directions. By integrating radially and scaling with the bulk velocity (U_b) and the pipe radius (R), one obtains

$$-\overline{u_r' u_z'}^{\dagger} + \frac{1}{\mathrm{Re}}\frac{dU^{\dagger}}{dr^{\dagger}} = \frac{f}{2}\left(1 - \frac{r}{R}\right). \tag{2}$$

Here, $f = 2\tau_w/\rho U_b^2$ represents the Fanning friction factor and the Reynolds number is defined as $\mathrm{Re} = 2U_b R/\nu$. The superscript † indicates the aforementioned scaling, τ_w represents the wall shear stress, and ν is the kinematic viscosity.

In a series of pioneering works, Gioia and Chakraborty [1–4] explored the link between turbulent energy spectrum and Reynolds stress ($\overline{u_r' u_z'}$). These works are based on a phenomenological model, in which on a hypothetical wet surface close to the wall, the net vertical momentum transfer balances the wall shear stress. Over this surface, the streamwise velocity scales with bulk velocity (U_b) and the normal velocity is induced by eddies striking on it [1]. Considering a dominant eddy (with the

*hamidreza@im.ufrj.br

size s proportional to the distance of the wet surface to the wall) responsible mainly for the normal velocity fluctuations, the wall shear stress can be approximated as $\tau_w \propto \rho u_s U_b$. The characteristic velocity of the dominant eddies, u_s, is then related to the turbulent energy spectrum as [1,2]

$$u_s^2 = \int_0^s E_{TKE}(\sigma)\sigma^{-2} d\sigma, \tag{3}$$

where $E_{TKE}(\sigma) = c_E \epsilon^{2/3}\sigma^{5/3} C_d(\eta/\sigma) C_e(\sigma/R)$ is the Kolmogorov spectrum with dissipative range (C_d) and energetic range (C_e) corrections, $\eta = \nu^{3/4}\epsilon^{-1/4}$ is the Kolmogorov length scale, and ϵ is the dissipation rate (see (1) for more details). For the smooth wall, Gioia and Chakraborty [1] proposed that $s \propto \eta$, where η was calculated using the bulk values ($\epsilon = U_b^3/R$). Omitting the effects of corrections (C_d, C_e), one can easily recover the well-known Blasius equation from this phenomenological model as

$$f = \frac{1}{4\pi}\,\mathrm{Re}^{-1/4}. \tag{4}$$

Inserting Eq. (4) into Eq. (2) over the wet surface ($r = s \propto \eta$), and neglecting the effects of the viscosity and distance from the wall for the high enough Reynolds numbers, one recovers

$$\overline{u_r' u_z'} \propto u_s U_b. \tag{5}$$

Assuming the validity of (5) on any layer far enough from the wall, the mean velocity profile (MVP) has also been investigated [2] using Eq. (1).

The model has been successfully extended to predict the friction factor in 2D turbulence [5–7], turbulent heat transfer [8], frictional losses in the presence of the permeable walls [9], purely viscous non-Newtonian fluids [10–12], and recently to the viscoelastic fluids [13].

Although it has been successfully extended into other types of turbulence, some questions regarding the underlying assumptions of this model are still remaining. For example, the relation between u_s and E_{TKE}, Eq. (3), is *ad hoc* [14]. The one-dimensional cospectrum $F_{u_r u_z}$, which connects u_r' and u_z' as

$$\overline{u_r' u_z'} = \rho \int_0^\infty F_{u_r u_z}(k) dk, \tag{6}$$

is the natural choice [14,15]. Then, the $-5/3$ spectral scaling exponent can be related to the $-7/3$ cospectral exponent [14]. One of the most important questions regards the wet surface. There is no experimental evidence about the existence of such a layer, scaling (wall distance) with the Kolmogorov's length scale. It is very important to notice that the Kolmogorov length scale in the final form of the Gioia and Chakraborty phenomenological model is based on the bulk velocity [1], not the local velocity at wet surface. One may argue, far enough from the wall, the mean velocity scales with the bulk velocity. However, the wet surface in the phenomenological model of Gioia and Chakraborty [1] is not far from the wall and does not satisfy this requirement. Also, at such a distance from the wall, the turbulent production and dissipation are widely separated. The latter has been used to calculate MVP in Ref. [2].

It was observed that this model cannot predict adequately the friction factor for high Reynolds numbers ($\mathrm{Re} > 10^5$), inside smooth conduits [16]. On the other hand, moving the wet surface to the mesolayer ($s \propto \mathrm{Re}_\tau^{1/2}$) permits the model to reproduce the observed friction factors very accurately [16] for extreme Reynolds numbers ($\mathrm{Re} > 10^6$). Based on this, the friction factor for the extreme Reynolds numbers was obtained as

$$f = \frac{2\tau_w}{\rho U_b^2} = C_e \mathrm{Re}_\tau^{-1/6}, \tag{7}$$

where $\mathrm{Re}_\tau = u_* R/\nu$ and $u_* = \sqrt{\tau_w/\rho}$. Figure 1 compares the predictions of Eqs. (4) and (7) with experimental data from Princeton Superpipe [17–19] and the Hi-Reff facility from the National

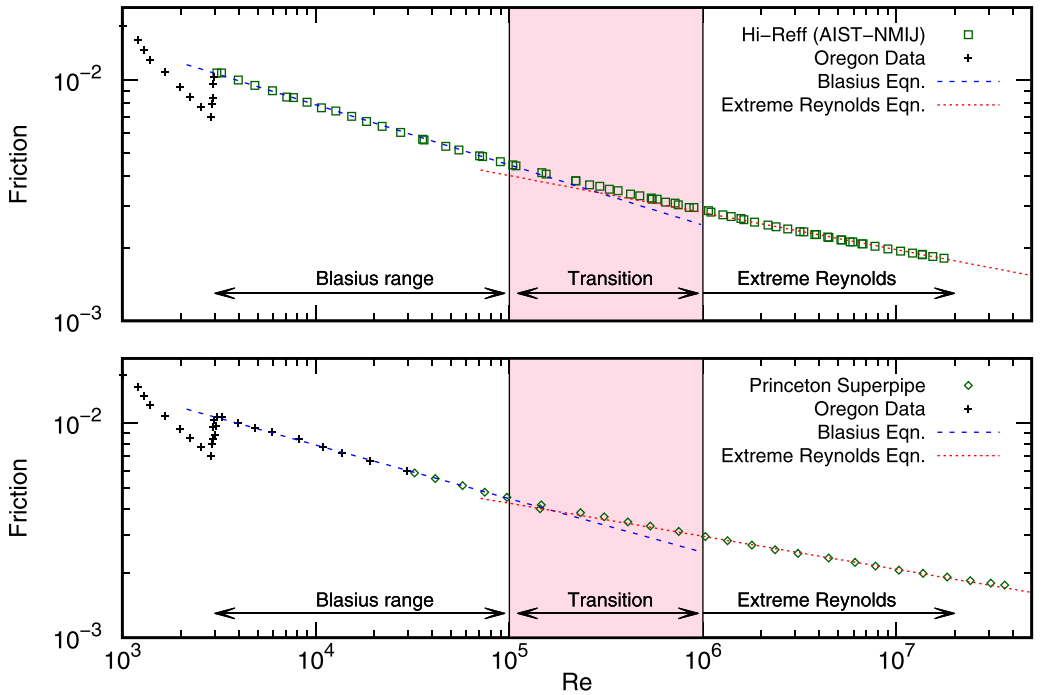

FIG. 1. Friction factor data for Hi-Reff (AIST-NMIJ) [20] and Princeton Superpipe [18] compared to Blasius' formula (4) and the extreme Reynolds friction formula (7) ($C_e = 2.359 \times 10^{-2}$ for Hi-Reff data and $C_e = 2.486 \times 10^{-2}$ for Superpipe data). To complete the figure, the experimental data from the Oregon smooth pipe experiment [22] for low to moderately high Reynolds numbers is also displayed here. Transition region is where the error of the predictions by Eqs. (4) or (7) are higher than 1%.

Metrology Institute of Japan (AIST/NMIJ) [20,21]. As evident, the turbulent friction factor experiences two extremes: the Blasius regime and the extreme Reynolds regime. The result of our previous work shows [16] that the accuracy of Eq. (7) in the latter regime is comparable to the Blasius equation (4), in its proper regime. Also, a transition region, between the Blasius and extreme Reynolds regimes ($10^5 < \mathrm{Re} < 10^6$) was observed [16]. Based on this work, while the prediction error in both the Blasius and extreme Reynolds regimes is less than 1% for both experiments, the error increases up to 8% in the transition region. The transition region is indicated by color in Fig. 1.

Our assumption about the location of the wet surface at extreme Reynolds numbers ($s \propto \mathrm{Re}_\tau^{1/2}$) represents a well-documented and experimentally observed layer. The $\mathrm{Re}_\tau^{1/2}$ scaling is associated with the location of the peak of Reynolds stress [23,24], the outer peak of the streamwise turbulence intensity [25], and the lower bound of the attached eddy region (logarithmic region) [26,27].

The present work explores the latter idea in more detail and examines the connection between the discussed phenomenological model [1] and the attached eddy hypothesis (AEH). As can be seen in Fig. 1, the transition between Eqs. (4) and (7) spans an order of magnitude (10^5–10^6). This transition could be tracked in other turbulent quantities. Yakhot *et al.* [28] showed that the area-averaged turbulent kinetic energy changes the scaling around $\mathrm{Re} = 10^5$. Wei [29] demonstrated that the turbulent kinetic energy production (or dissipation), from the wall to the peak of Reynolds stress and from the latter point to the pipe center, reaches an equilibrium after $\mathrm{Re} = 10^5$. de Giovanetti *et al.* [30] identified that after $\mathrm{Re}_\tau > 2000$ ($\mathrm{Re} \approx 10^5$), the main contribution to the skin friction comes from the self-similar energy-containing motions. The striking point about the mentioned transitions is that they all start around $\mathrm{Re} = 10^5$ (the end of the Blasius regime in Fig. 1) and almost instantaneously a new scaling appears. This is in contrast to the results shown in Fig. 1, where the

transition happens over an order of magnitude. The main motivation behind the present work is to resolve this discrepancy.

In what follows, first a reformulation of the phenomenological model [1] is proposed which is compatible with AEH. Then by connecting the lower bound of the logarithmic region to the wet surface, a revised version of the extreme Reynolds friction equation is derived, which shows superior accuracy in the transition region. This new equation, in contrast to Eq. (7), behaves like a continuous extension of the Blasius equation. Then this new friction equation is used to obtain a MVP for the post-Blasius regime.

II. FRICTION AND ATTACHED EDDIES

The phenomenological model of the Gioia and Chakraborty [1] shares similarities with the attached eddy hypothesis (AEH) by Townsend [31]. This hypothesis considers the existence of a layer with constant Reynolds stress ($\overline{u_r' u_z'}$), where the flow could be considered as a random superposition of energy-containing self-similar wall-attached eddies and a background flow. The constant stress layer is assumed to be located where one could ignore the viscous length scale ν/u_* with respect to the wall distance [32]. These eddies have an identical (shape) velocity field with a common velocity scale, but a different unspecified length scale. The constant stress layer limits the size distribution of eddies, which results in a well-known logarithmic mean velocity profile, logarithmic streamwise and spanwise turbulent intensities, and other distributions in a constant stress layer [26,32–35]. Another important implication of the mentioned size distribution is the invariance of the turbulent dissipation along the constant stress layer [34]. We will return to this point later.

The limits of the logarithmic layer could be defined as the region where both mean axial velocity and turbulent intensity follows a logarithmic behavior [26]. Such analysis over different canonical turbulent flows indicates that the upper limit of the logarithmic layer is in the order of the geometrical characteristic length scale of the system [26] ($0.1R$ to $0.2R$ for the pipe flow). For the lower limit l, Marusic and co-workers [26,27] proposed $l^+ \propto \mathrm{Re}_\tau^{1/2}$ dependence, which is in agreement with the modification of the AEH proposed by Eynik [36] to account for the viscous effects near the wall (the superscript $+$ represents the usual wall scaling). A conservative estimate as $l^+ = 3\sqrt{\mathrm{Re}_\tau}$ is given by Marusic *et al.* [26] for the lower bound of the logarithmic region, which compares reasonably with the location of the outer peak in streamwise turbulent intensity [25] ($y_{op}^+ = 3.9\sqrt{\mathrm{Re}_\tau}$).

Thus, it is obvious that the logarithmic region (or attached eddies) is located further from the wall so that it is under the influence of the core flow. Therefore, it is reasonable to assume that the axial mean velocity (background flow in AEH) in this region scales with the bulk velocity U_b. This assumption is supported by Wei *et al.* [37] where it was observed that near the maximum Reynolds stress location, the region where the pressure and viscous forces balance each other, the bulk velocity scales as $U_b \approx 0.5U_c$. Also considering the invariance of the turbulent dissipation rate in this region and the fact that the outer limit scales with the large scale motions, one could approximate the dissipation rate at the lower limit as $\epsilon \propto U_b^3/R$. Therefore, the characteristic velocity (u_l) for the attached eddies at the lower limit of the logarithmic region scales as

$$\frac{u_l}{U_b} \propto \left(\frac{l}{R}\right)^{1/3} = \mathrm{Re}_\tau^{-1/6}. \tag{8}$$

The same conclusion can be drawn by using Eq. (3). In this case, because of the location of the wetsurface, the dissipative and energetic corrections are irrelevant.

If one moves the wet surface in the phenomenological model [1] to the lower bound of the logarithmic layer, the aforementioned issues of the phenomenological model of Gioia and Chakraborty [1] could be avoided. Using the new location of the wet surface, the Reynolds stress, Eq. (5), could be replaced by

$$\overline{u_r' u_z'} \propto u_l U_b. \tag{9}$$

Also, it must be emphasized here that the new wet surface is much farther from the wall than the same surface in the original phenomenological model (scaled with Kolmogorov's length scale). Therefore, the effect of r/R on the right hand side of Eq. (2) can no longer be neglected ($r/R = C_l\,\mathrm{Re}_\tau^{-1/2}$), at least in lower Reynolds numbers. Here, C_l dictates the exact position of the lower limit, which will be discussed later.

To complete our discussion, one needs to provide an approximation for the viscous term in (2). It is important to notice that the lower bound of the attached eddy region is inside the third layer of the four-layer structure proposed by Wei *et al.* [37]. This structure characterizes different regions of the turbulent flow by a predominance of two of the three terms (Reynolds force, viscous force, and pressure force) in Eq. (1). In the third layer, viscous force balances the pressure force. The spatial limits of this layer scale with $\mathrm{Re}_\tau^{1/2}$ and the maximum Reynolds stress also happens inside it. Wei *et al.* [37] also showed

$$\frac{dU^+}{dy^+} = \mathcal{O}\left(\mathrm{Re}_\tau^{-1/2}\right), \tag{10}$$

in the third layer. Considering wet surface inside this layer or very close to it, one can approximate the viscous term as

$$\frac{1}{\mathrm{Re}}\frac{dU^\dagger}{dy^\dagger} = \frac{u_*^2}{U_b^2}\frac{dU^+}{dy^+} = \left(\frac{f}{2}\right)C_u\mathrm{Re}_\tau^{-1/2}. \tag{11}$$

Based on our model, the attached eddies striking on the wet surface are the dominant mechanism to produce the Reynolds stress at this layer. However, the viscous term is governed by the background flow of these eddies in the AEH.

Finally, introducing Eqs. (9) and (11) into Eq. (2) results in

$$f = C_k\frac{\mathrm{Re}_\tau^{-1/6}}{1 - C_b\,\mathrm{Re}_\tau^{-1/2}}, \tag{12}$$

where $C_b = C_l + C_u$ and C_k is the proportionally constant. Both constants will be adjusted using experimental data.

In this work, for the analysis of extreme Reynolds numbers flows, the experimental data from the Hi-Reff facility obtained from the National Metrology Institute of Japan (AIST/NMIJ), [20,21] as well as data from the Princeton Superpipe [17–19] are considered. Experimental data from the Oregon smooth pipe experiment [22] is also provided for low to moderately high Reynolds numbers.

McKeon and co-workers [18,19] provided the following friction factor relation:

$$\frac{1}{\sqrt{f}} = 1.930\log_{10}\mathrm{Re}\sqrt{f} - 0.537, \tag{13}$$

based on the Princeton Superpipe data. Further analysis of these data shows that for $\mathrm{Re} > 1.7\times10^7$, either the pipe surface can no longer be considered as hydraulically smooth or the extrapolation of the static pressure correction is incorrect [38]. Therefore, as a reminder, only Reynolds numbers less than this limit are considered.

Considering the Hi-Reff facility data, Furuichi *et al.* [20] estimated the following friction equation for the range $1.2\times10^4 \leqslant \mathrm{Re} \leqslant 1.8\times10^7$:

$$\frac{1}{\sqrt{f}} = 2.090\log_{10}\mathrm{Re}\sqrt{f} - 1.172. \tag{14}$$

Again it has been argued that the roughness effects can be relevant for $\mathrm{Re} > 1.0\times10^7$.

It must be emphasized here that the differences between the friction factors obtained in these two experiments (Hi-Reff and Superpipe) reach up to 6% for high Reynolds numbers. The roughness effects at high Reynolds numbers could be likely the main source of this discrepancy [20]. For such extreme Reynolds numbers, the characteristic scales of the turbulent flow can be sufficiently small

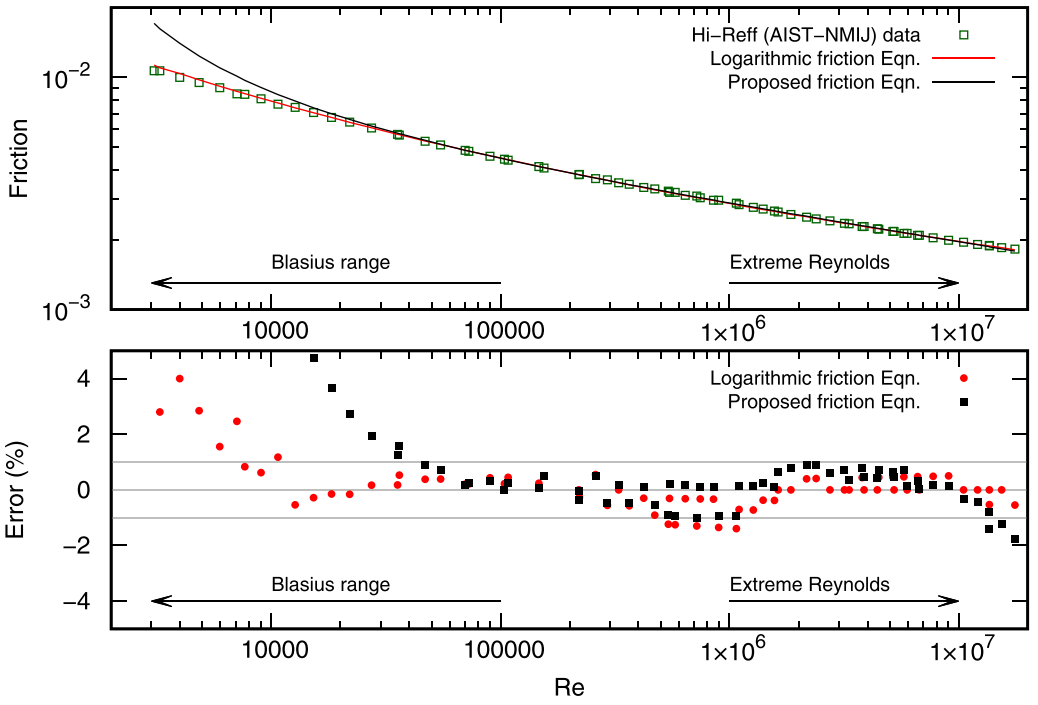

FIG. 2. Comparison of the friction factor data for Hi-Reff (AIST-NMIJ) [20] with the proposed formula (12), and the logarithmic law (14). (top) friction factor, (bottom) deviation of the predicted values from the experimental data.

so that the assumption of hydraulic smoothness for the pipe is no longer valid. This significant difference between two data sets is the reason why the fitting process has been done separately for each experiment below.

Equation (12) is calibrated for the both experimental data sets mentioned above. For the Hi-Reff data, the constants are $C_k = 1.4268 \times 10^{-2}$ and $C_b = 5.96$, while for the Superpipe data, they are $C_k = 1.5 \times 10^{-2}$ and $C_b = 4.2$. These constants were adjusted for Reynolds numbers from 10^5 to 10^7, while the friction data above and below this range were discarded from the fitting procedure as they may be influenced by roughness [18,19] or be in the Blasius range. These constants (specifically C_k) differ by approximately 5%, which reflects the differences between the data sets, as mentioned before.

Figures 2 and 3 show the difference between Eq. (12) and the experimental data. As evident, the new equation predicts the friction factor with less than a 1% error, starting from Reynolds number slightly less than 10^5 (in the Blasius regime) to values as high as $\mathrm{Re} = 10^7$. In these figures, the experimental data also have compared with logarithmic laws of Eqs. (14) and (13). Our results show that the accuracy of the proposed equation is similar to these logarithmic friction laws. Comparing to the extreme friction equation (7), Eq. (12) extends the domain of applicability of the former at least one order of magnitude.

We end this section with an important remark concerning the relation between the fitted constants and the log law. Although our model does not depend on the logarithmic velocity profile, one could use logarithmic profile to calculate the velocity derivative in Eq. (11) as

$$\left.\frac{dU^+}{dy^+}\right|_{y^+=l^+} = \frac{1}{\kappa\, l^+} = \frac{1}{\kappa\, C_l}\,\mathrm{Re}_\tau^{-1/2}, \tag{15}$$

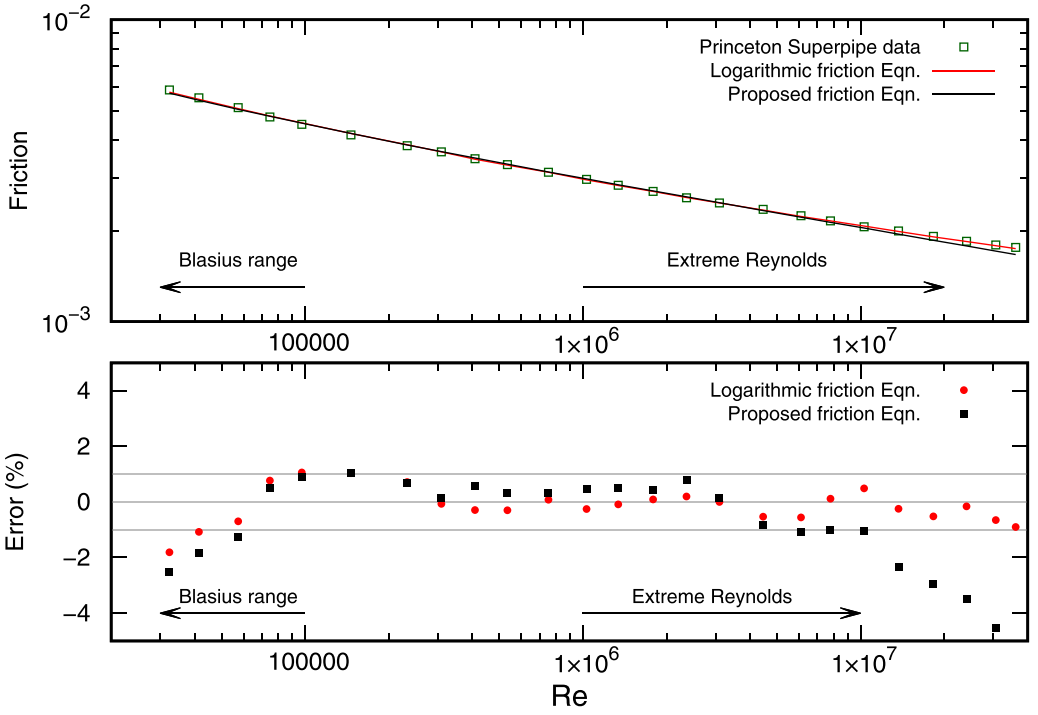

FIG. 3. Comparison of the friction factor data for Princeton Superpipe [18] with the proposed formula (12), and the logarithmic law (13). Top: friction factor, Bottom: deviation of the predicted values from the experimental data.

where κ is von Karman's constant. Comparing the later equation with Eq. (11) shows $C_u = (\kappa\, C_l)^{-1}$, and therefore $C_b = C_l + (\kappa\, C_l)^{-1}$. Considering $\kappa = 0.4$ and $C_l = 3$ (a conservative approximation for the lower bound of the logarithmic layer [26]), one obtains $C_b = 3.84$, while $C_l = 3.9$ and $\kappa = 0.385$ would result in $C_b = 4.54$. These are in agreement with the values obtained from the calibration process above ($C_b = 5.96$ for the Hi-Reff data and $C_b = 4.2$ for the Superpipe data).

In fact, one could also use the calibrated C_b to calculate the exact location of the wet surface. Considering $\kappa = 0.385$ for the Hi-Reff data [20], the constant can be calculated as $C_l = 5.48$. For the Princeton Superpipe data [18] with $\kappa = 0.421$, one obtains $C_l = 3.52$. Both values are very close to the limits for the lower bound of the logarithmic region as discussed before.

III. MEAN VELOCITY PROFILE

This section discusses the effect of the transition between Blasius and extreme Reynolds regimes on the mean velocity profile. The MVP at extreme Reynolds numbers has been analyzed before, considering the incomplete similarity in inner variables at the core region of the flow [39]. In this section, the MVP is studied based on the asymptotic complete similarity in inner scaling.

From dimensional arguments, the MVP can be written as $U = f(r; R, \nu, \tau_w)$. Using inner scaling one finds

$$U^+ = \Phi\left(\frac{y}{\delta_\nu}, \frac{y}{R}\right) = \Phi\left(y^+, \frac{y^+}{\mathrm{Re}_\tau}\right). \tag{16}$$

In the limit of high Reynolds number ($\mathrm{Re}_\tau \gg 1$), one can assume that there is a region where $y^+/\mathrm{Re}_\tau \approx 0$, and therefore the velocity is only a function of y^+, as $U^+ = \Phi(y^+)$. The attached

eddy region discussed in the previous section can be also considered as the limits where the latter assumption is valid. However, this assumption breaks by approaching the core flow. By integrating the MVP, the bulk velocity can be obtained as

$$U_b^+ = \frac{2\alpha}{\mathrm{Re}_\tau^2}\int_0^{Re_\tau}(\mathrm{Re}_\tau - y^+)\Phi(y^+)dy^+, \tag{17}$$

where $U_b^+ = U_b/u_* = (f/2)^{-1/2}$. The assumed velocity profile works for a limited range of y^+ inside a pipe. In particular, it is not a good approximation for the core flow. In Eq. (17), α stands for the corrections related to the latter region. It is possible to use Eq. (12) to calculate U_b^+,

$$U_b^+(Re_\tau) = \left(\frac{C_k}{2}\right)^{-1/2}\mathrm{Re}_\tau^{1/12}\left(1 - C_b\mathrm{Re}_\tau^{-1/2}\right)^{1/2}. \tag{18}$$

Considering that the integral in Eq. (17) represents the convolution and by using Laplace transform, it is easy to show that

$$\Phi(y^+) = \frac{1}{2\alpha}\frac{d^2}{d\,y^{+2}}[U_b^+(y^+)y^{+2}], \tag{19}$$

which implies

$$\Phi(y^+) = \frac{1}{2\alpha}\left(\frac{C_k}{2}\right)^{-1/2}\frac{d^2}{d\,y^{+2}}\left[y^{+25/12}\left(1 - C_b y^{+-1/2}\right)^{1/2}\right].$$

For the Princeton Superpipe data [18], if the constants obtained in the previous section are used, one has $(C_k/2)^{-1/2} = 11.54$. By adjusting with the experimental observations, the correction factor can be calculated as $\alpha = 1.0167$, which is very minute. The famous Prandtl power-law profile, $U^+ = C_p\, y^{+1/7}$, can be obtained using the same method, by replacing the Blasius equation (4) with Eq. (12) in (17). Following the same steps as above results in $(C_k/2)^{-1/2} = 8.57$ and $\alpha = 1.026$. In the term of the Prandtl profile, this is equivalent to $C_p = 8.35$, while the suggested value by Prandtl is $C_p = 8.7$. As Prandtl noted, this power-law profile provides a good approximation up to $\mathrm{Re} = 10^5$.

Figure 4 compares the experimental MVPs for the Princeton Superpipe data [18] with profile (19) and Prandtl's profile, for different Reynolds numbers. The empirically obtained logarithmic profile by McKeon *et al.* [18],

$$U^+ = \frac{1}{0.421}\ln(y^+) + 5.6, \tag{20}$$

is also provided in this figure for comparison. This log law is precise for $600 < y^+ < 0.12R^+$ [18].

As evident in Fig. 4, at low Reynolds numbers the Prandtl power law is a better fit rather than Eq. (19) or Eq. (20). However, by increasing the Reynolds number, the MVP gradually shifts toward the new profile (19), and at ultimate Reynolds numbers the new profile is a better approximation. The left hand side of Fig. 4 shows a deviation of the MVPs from the experimental data. This clearly demonstrates that Prandtl's profile and Eq. (19) predict the velocity profile very accurately in both ends of the studied range. These results suggest that the MVP of Eq. (19) is good a approximation for $\mathrm{Re} > 10^6$. In these figures, the colored region indicates $600 < y^+ < 0.12R^+$, where the logarithmic law (20) is found reliable [18]. By increasing Reynolds number, the new profile (19) and Eq. (20) become indistinguishable in this region.

The same calculations for the Hi-Reff data results in $\alpha \approx 1.0$. Figure 5 compares the experimental MVPs of [21] with Eq. (19). This figure also contains the following empirical logarithmic law by Furuichi *et al.* [21]:

$$U^+ = \frac{1}{0.382}\ln(y^+) + 4.4, \tag{21}$$

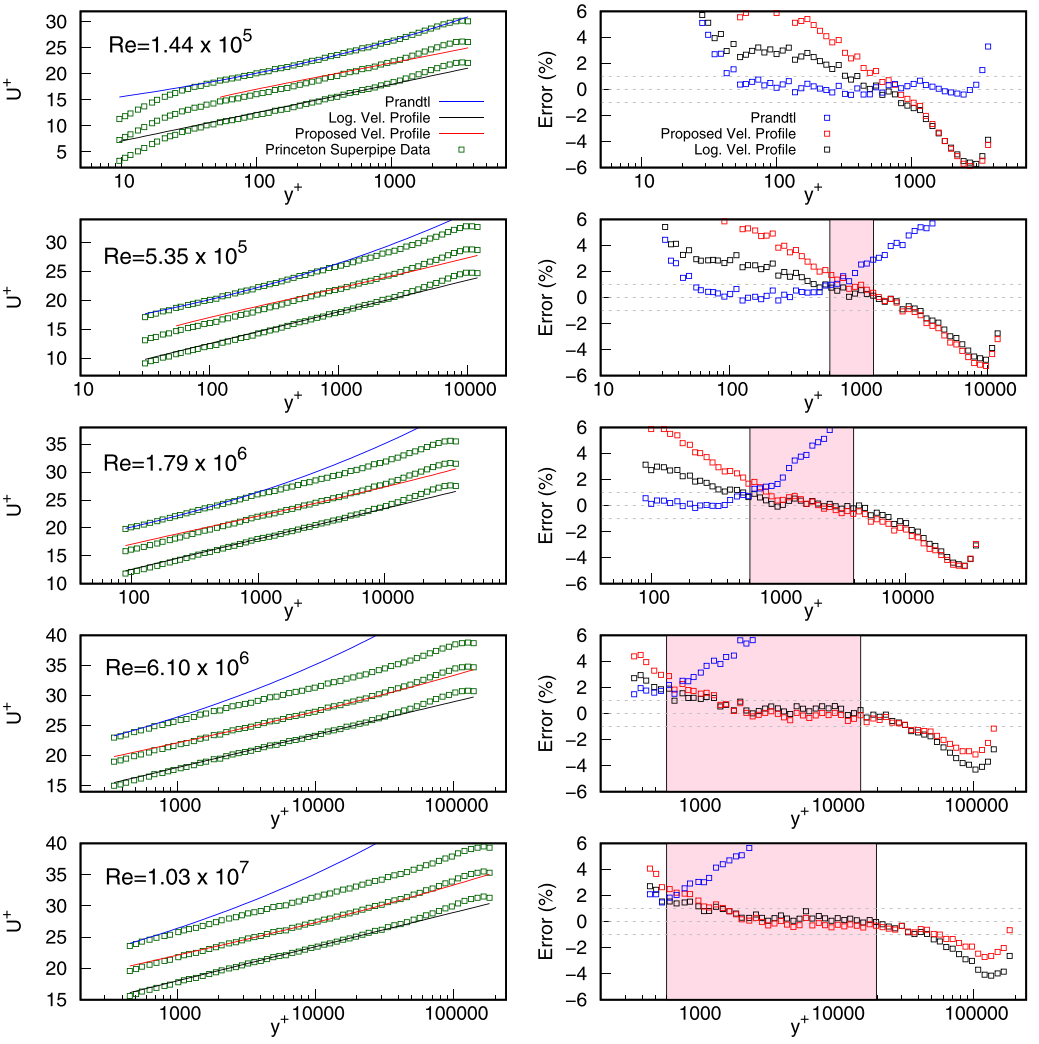

FIG. 4. Comparison of the Superpipe velocity profiles with the logarithmic velocity profile of (20), Prandtl's power law ($U^+ \propto y^{+1/7}$), and the proposed velocity profile of (19). Left: velocity profiles; right: deviation from the experimental data. The colored region indicates $600 < y^+ < 0.12R^+$.

which was determined to be accurate for $3\mathrm{Re}_\tau^{0.5} < y^+ < 0.2\mathrm{Re}_\tau$. The pink region in this figure indicated the latter range. The same as the Princeton Superpipe data, it is clearly visible that Eq. (19) has the same accuracy as the logarithmic law for $\mathrm{Re} \geqslant 10^6$. Also it is very interesting to note that the validity region provided for Eq. (21) coincides with the lower and upper limits of the attached eddies that our theory is based on.

Under an incomplete similarity assumption, Barenblatt [40] argued that the velocity profile can be approximated as $U^+ = \beta y^{+\gamma}$, where β and γ are functions of the Reynolds number. In the limit of very high Reynolds numbers, Eq. (12) reduces to $f \propto \mathrm{Re}_\tau^{-1/6}$. As a result, the velocity profile of (19) simplifies to $U^+ \propto y^{+1/12}$. This is in total agreement with the proposed power-law profiles in the literature, as shown in Fig. 6. In this figure, some available approximations of the exponent [41–43] (γ) are compared with the two limits discussed above ($1/7$ for the Blasius regime and $1/12$ for the extreme Reynolds numbers). As can be seen, the latter exponent acts as an an asymptotic limit in the extreme Reynolds numbers.

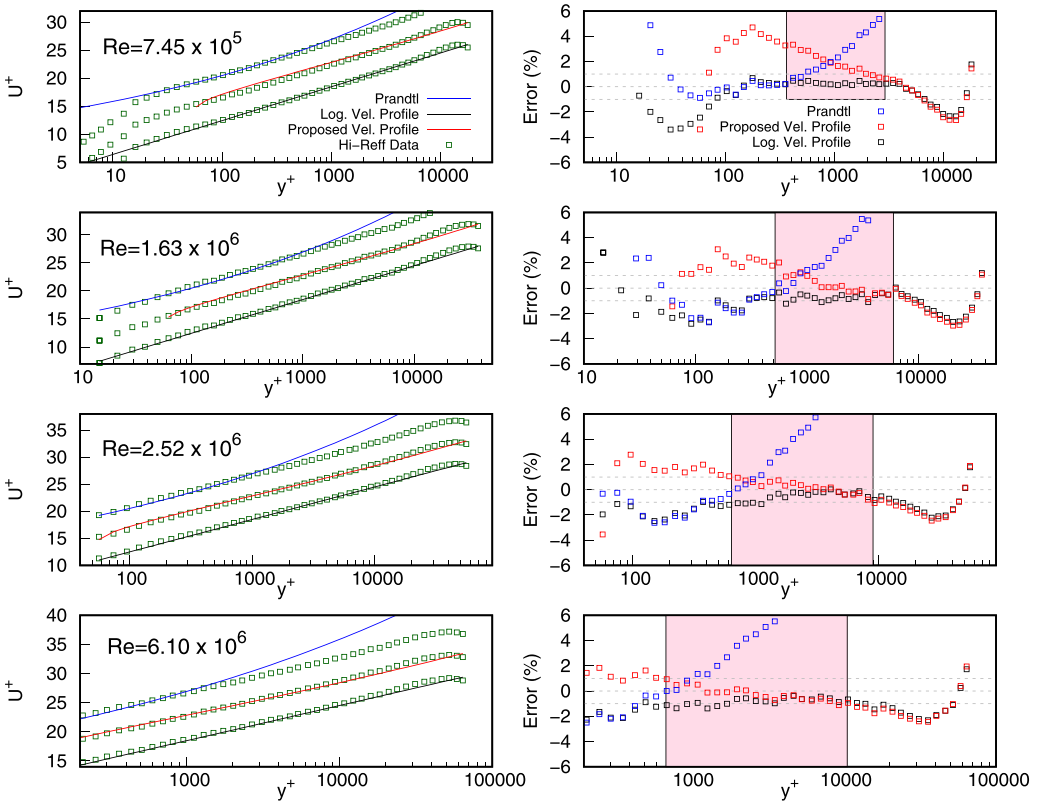

FIG. 5. Comparison of the Hi-Reff velocity profiles with the logarithmic velocity profile of (21), Prandtl's power law ($U^+ \propto y^{+1/7}$), and the proposed velocity profile of (19). Left: velocity profiles; right: deviation from the experimental data. The colored region indicates $3\sqrt{R^+} < y^+ < 0.2R^+$.

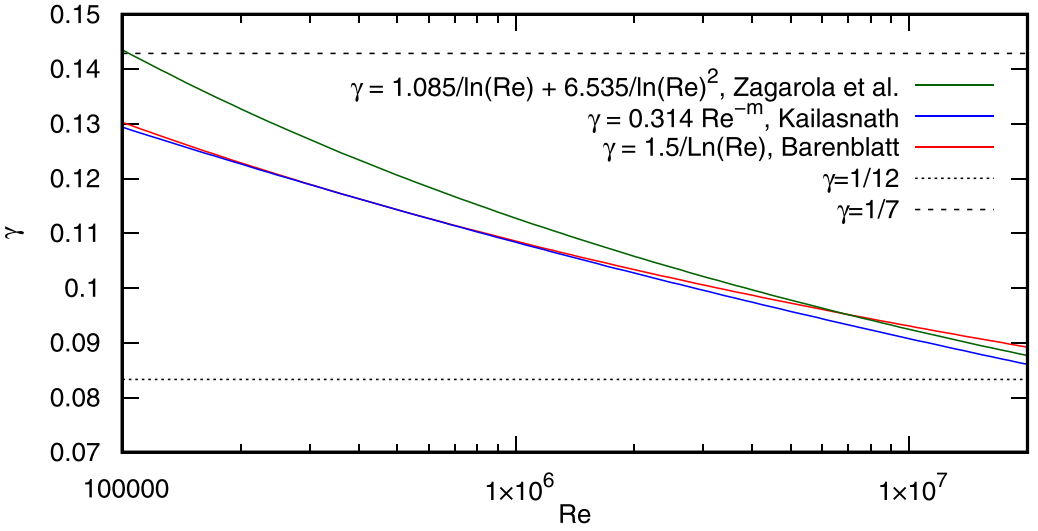

FIG. 6. Comparing different exponents γ of the power-law mean velocity profile $U^+ = \beta y^{+\gamma}$ from Barenblatt [41], Kailasnath [42], and Zagarola *et al.* [43]. The Prandtl's power-law ($\frac{1}{7}$) and extreme Reynolds number ($\frac{1}{12}$) exponents are shown as the limits.

As is evident throughout this work, the developed friction equation (12) and the mean velocity profile (19) show similar behavior as the logarithmic friction equations and velocity profiles in the range $10^5 < \mathrm{Re} < 10^7$.

IV. CONCLUSION

In the present work, the phenomenological model of Gioia and Chakraborty [1] is modified by moving the wet surface from a hypothetical layer (with distance from the wall proportional to Kolmogorov's length scale) to the lower bound of the attached eddies region. Although there are other works [44] exploring the relation between the spectral model of Gioia and Chakraborty [1] and the AEH [31], the present study provides evidence for the existence of such layer and its implications in high Reynolds numbers. The lower bound of the attached eddies is far enough from the wall to fulfill assumptions in the original phenomenological model.

Other studies support our model. It has been observed that the near-wall motions lose their importance in friction generation by increasing Reynolds numbers, while the large scale motions have limited importance [30]. On the other hand, the friction is mainly generated by the self-similar motions in the logarithmic region [30,45].

As shown, the new phenomenological model predicts the friction factor successfully, starting right after the end of the Blasius regime. This is in accordance with the emergence of this transition, which happens at the same Reynolds number almost instantaneously [28,29]. Also, the effect of this transition in the mean velocity profile is demonstrated in this work. It observed that by increasing Reynolds number, a change in the exponent of the power-law type mean velocity profile will be experienced. We conjecture that for high enough Reynolds numbers, both power-law profiles, Eq. (19) and Prandtl's power-law profile, will simultaneously approximate different regions of the mean velocity profile. In this case, the Prandtl profile collapses on MVP in lower y^+ and the new power-law formula matches the profile farther from the wall. A similar observation has been reported before [18], where a power-law region, $U^+ \propto y^{+0.142}$, was observed near the wall, and followed by a logarithmic region afterward for $\mathrm{Re} > 2 \times 10^5$. Unfortunately, the experiments cannot properly resolve the flow field very close to the wall at high Reynolds numbers, while the direct numerical simulation are far from the extreme Reynolds range. Therefore, verification of this conjecture is not possible now. It is also possible that the so-called low-Reynolds effects in determining the von Kármán constant results from the switch between two profiles.

Returning to the original model, we believe the existence of the wet surface in the Blasius regime, with distance from the wall proportional to Kolmogorov's length scale [1,2], is questionable. New studies suggest that at lower Reynolds numbers, wall-incoherent motions made up of Kolmogorov-type fine scales and other wall-detached motions become important [46,47]. Extended attached eddy models such as the one proposed by Chandran *et al.* [47] could help to enhance the phenomenological model and answer questions related to it in the Blasius regime.

Finally, much evidence indicates that the transition occurs near $\mathrm{Re} = 10^5$. The mechanism of this transition is unknown, and the understanding of it is crucial for further progress. Also, the roughness could affect the turbulent flow differently after and before the transition, a matter which need further research.

[1] G. Gioia and P. Chakraborty, Turbulent Friction in Rough Pipes and the Energy Spectrum of the Phenomenological Theory, Phys. Rev. Lett. **96**, 044502 (2006).

[2] G. Gioia, N. Guttenberg, N. Goldenfeld, and P. Chakraborty, Spectral Theory of the Turbulent Mean-Velocity Profile, Phys. Rev. Lett. **105**, 184501 (2010).

[3] C. Zuniga Zamalloa, H. C.-H. Ng, P. Chakraborty, and G. Gioia, Spectral analogues of the law of the wall, the defect law and the log law, J. Fluid Mech. **757**, 498 (2014).

[4] G. Gioia and P. Chakraborty, Spectral derivation of the classic laws of wall-bounded turbulent flows, Proc. R. Soc. London, Ser. A **473**, 20170354 (2017).
[5] N. Guttenberg and N. Goldenfeld, Friction factor of two-dimensional rough-boundary turbulent soap film flows, Phys. Rev. E **79**, 065306(R) (2009).
[6] H. Kellay, T. Tran, W. Goldburg, N. Goldenfeld, G. Gioia, and P. Chakraborty, Testing a Missing Spectral Link in Turbulence, Phys. Rev. Lett. **109**, 254502 (2012).
[7] A. Vilquin, J. Jagielka, S. Djambov, H. Herouard, P. Fischer, C.-H. Bruneau, P. Chakraborty, G. Gioia, and H. Kellay, Asymptotic turbulent friction in 2d rough-walled flows, Sci. Adv. **7**, eabc6234 (2021).
[8] L. Ventola, F. Robotti, M. Dialameh, F. Calignano, D. Manfredi, E. Chiavazzo, and P. Asinari, Rough surfaces with enhanced heat transfer for electronics cooling by direct metal laser sintering, Int. J. Heat Mass Transfer **75**, 58 (2014).
[9] C. Manes, L. Ridolfi, and G. Katul, A phenomenological model to describe turbulent friction in permeable-wall flows, Geophys. Res. Lett. **39**, L14403 (2012).
[10] H. R. Anbarlooei, D. O. A. Cruz, F. Ramos, and A. P. Silva Freire, Phenomenological Blasius-type friction equation for turbulent power-law fluid flows, Phys. Rev. E **92**, 063006 (2015).
[11] H. R. Anbarlooei, D. O. A. Cruz, F. Ramos, C. M. M. Santos, and A. P. Silva Freire, Phenomenological friction equation for turbulent flow of Bingham fluids, Phys. Rev. E **96**, 023107 (2017).
[12] H. Anbarlooei, D. Cruz, F. Ramos, C. Santos, and A. S. Freire, On the connection between Kolmogorov microscales and friction in pipe flows of viscoplastic fluids, Physica D (Amsterdam, Neth.) **376-377**, 69 (2018), special Issue: Nonlinear Partial Differential Equations in Mathematical Fluid Dynamics.
[13] H. Anbarlooei, D. Cruz, and F. Ramos, A phenomenological equation for the friction factor of turbulent flow of viscoelastic fluids: From the newtonian to the maximum drag reduction regime, in *25th International Congress of Theoretical and Applied Mechanics* (IUTAM, Milan, 2021).
[14] G. G. Katul and C. Manes, Cospectral budget of turbulence explains the bulk properties of smooth pipe flow, Phys. Rev. E **90**, 063008 (2014).
[15] D. Li and G. G. Katul, On the linkage between the k-5/3 spectral and k-7/3 cospectral scaling in high-Reynolds number turbulent boundary layers, Phys. Fluids **29**, 065108 (2017).
[16] H. Anbarlooei, D. Cruz, and F. Ramos, New power-law scaling for friction factor of extreme Reynolds number pipe flows, Phys. Fluids **32**, 095121 (2020).
[17] M. V. Zagarola and A. J. Smits, Mean-flow scaling of turbulent pipe flow, J. Fluid Mech. **373**, 33 (1998).
[18] B. J. Mckeon, J. Li, W. Jiang, J. F. Morrison, and A. J. Smits, Further observations on the mean velocity distribution in fully developed pipe flow, J. Fluid Mech. **501**, 135 (2004).
[19] B. J. McKeon, M. V. Zagarola, and A. J. Smits, A new friction factor relationship for fully developed pipe flow J. Fluid Mech. **538**, 429 (2005).
[20] N. Furuichi, Y. Terao, Y. Wada, and Y. Tsuji, Friction factor and mean velocity profile for pipe flow at high Reynolds numbers, Phys. Fluids **27**, 095108 (2015).
[21] N. Furuichi, Y. Terao, Y. Wada, and Y. Tsuji, Further experiments for mean velocity profile of pipe flow at high Reynolds number, Phys. Fluids **30**, 055101 (2018).
[22] C. J. Swanson, B. Julian, G. G. Ihas, and R. J. Donnelly, Pipe flow measurements over a wide range of Reynolds numbers using liquid helium and various gases, J. Fluid Mech. **461**, 51 (2002).
[23] J. Klewicki, J. Philip, I. Marusic, K. Chauhan, and C. Morrill-Winter, Self-similarity in the inertial region of wall turbulence, Phys. Rev. E **90**, 063015 (2014).
[24] J. Klewicki and M. Oberlack, Finite Reynolds number properties of a turbulent channel flow similarity solution, Phys. Fluids **27**, 095110 (2015).
[25] R. Mathis, N. Hutchins, and I. Marusic, Scaling of inner and outer regions for flat plate boundary layers, *14th Australasian Fluid Mechanics Conference* (The University of Auckland, Auckland, New Zealand, 2010).
[26] I. Marusic, J. P. Monty, M. Hultmark, and A. J. Smits, On the logarithmic region in wall turbulence, J. Fluid Mech. **716**, R3 (2013).
[27] M. Samie, I. Marusic, N. Hutchins, M. K. Fu, Y. Fan, M. Hultmark, and A. J. Smits, Fully resolved measurements of turbulent boundary layer flows up to $\mathrm{Re}_\tau = 20\,000$, J. Fluid Mech. **851**, 391 (2018).

[28] V. Yakhot, S. C. C. Bailey, and A. J. Smits, Scaling of global properties of turbulence and skin friction in pipe and channel flows, J. Fluid Mech. **652**, 65 (2010).
[29] T. Wei, Integral properties of turbulent-kinetic-energy production and dissipation in turbulent wall-bounded flows, J. Fluid Mech. **854**, 449 (2018).
[30] M. de Giovanetti, Y. Hwang, and H. Choi, Skin-friction generation by attached eddies in turbulent channel flow, J. Fluid Mech. **808**, 511 (2016).
[31] A. A. Townsend, *The Structure of Turbulent Shear Flow*, 2nd ed. (Cambridge University Press, Cambridge, 1976).
[32] A. E. Perry and I. Marušić, A wall-wake model for the turbulence structure of boundary layers. Part 1. Extension of the attached eddy hypothesis, J. Fluid Mech. **298**, 361 (1995).
[33] J. D. Woodcock and I. Marusic, The statistical behaviour of attached eddies, Phys. Fluids **27**, 015104 (2015).
[34] H. Mouri, Two-point correlation in wall turbulence according to the Attached-Eddy hypothesis, J. Fluid Mech. **821**, 343 (2017).
[35] I. Marusic and J. P. Monty, Attached Eddy model of wall turbulence, Annu. Rev. Fluid Mech. **51**, 49 (2019).
[36] G. L. Eyink, Turbulent flow in pipes and channels as cross-stream "inverse cascades" of vorticity, Phys. Fluids **20**, 125101 (2008).
[37] T. Wei, P. Fife, J. Klewicki, and P. McMurtry, Properties of the mean momentum balance in turbulent boundary layer, pipe and channel flows, J. Fluid Mech. **522**, 303 (2005).
[38] B. J. McKeon and A. J. Smits, Static pressure correction in high Reynolds number fully developed turbulent pipe flow, Meas. Sci. Technol. **13**, 1608 (2002).
[39] G. Sanfins, H. R. Anbarlooei, D. O. A. Cruz, and F. Ramos, Complete and incomplete similarity for the mean velocity profile of turbulent pipe and channel flows at extreme Reynolds number, Phys. Fluids **33**, 085118 (2021).
[40] G. I. Barenblatt, *Scaling*, Cambridge Texts in Applied Mathematics (Cambridge University Press, Cambridge, UK, 2003).
[41] G. I. Barenblatt, A. J. Chorin, and V. M. Prostokishin, Scaling laws for fully developed turbulent flow in pipes: Discussion of experimental data, Proc. Natl. Acad. Sci. USA **94**, 773 (1997).
[42] P. Kailasnath, Reynolds Number Effects and the Momentum Flux in Turbulent Boundary Layers, Ph.D. thesis, Yale University, 1993.
[43] M. V. Zagarola, A. E. Perry, and A. J. Smits, Log laws or power laws: The scaling in the overlap region, Phys. Fluids **9**, 2094 (1997).
[44] B. Birnir, L. Angheluta, J. Kaminsky, and X. Che, Spectral link of the generalized Townsend-Perry constants in turbulent boundary layers, Phys. Rev. Research **3**, 043054 (2021).
[45] N. Renard and S. Deck, A theoretical decomposition of mean skin friction generation into physical phenomena across the boundary layer, J. Fluid Mech. **790**, 339 (2016).
[46] L. Agostini and M. Leschziner, Spectral analysis of near-wall turbulence in channel flow at $\mathrm{Re}_\tau = 4200$ with emphasis on the attached-eddy hypothesis, Phys. Rev. Fluids **2**, 014603 (2017).
[47] D. Chandran, J. P. Monty, and I. Marusic, Spectral-scaling-based extension to the attached Eddy model of wall turbulence, Phys. Rev. Fluids **5**, 104606 (2020).